ACS APPLIED MATERIALS & INTERFACES

Research Article

www.acsami.org

Construction of Sole Benzene Ring Porous Aromatic Frameworks and Their High Adsorption Properties

Lina Li, Kun Cai, Pengyuan Wang, Hao Ren,* and Guangshan Zhu

State Key Laboratory of Inorganic Synthesis and Preparative Chemistry, Jilin University, Changchun, China

Supporting Information

ABSTRACT: Porous organic frameworks (POFs), with their excellent performance in catalysis, electricity, sensor, gas storage, and separation, have attracted a great deal of attention from researchers all over the world. Generally, the monomers of POF materials require a rigid three-dimensional molecule configuration together with special functional groups, as well as being triggered by noble metal catalysts. Here we report a low-cost and easy-construction strategy for synthesizing PAF materials. A series of flat multi-benzene compounds are selected as building units, and those phenyl rings could couple together to form polymeric skeletons. The BET surface areas of resulting PAFs are moderate, ranging from 777 to 972 $m^2 g^{-1}$. However, they unexpectedly exhibit superior gas sorption capacities. At 1.0 bar and 77 K, the H_2 uptake of PAF-48 reaches 215 $cm^3 g^{-1}$. In addition, PAF-49 shows excellent performance in carbon dioxide and methane sorption, with values of 104 and 35 $cm^3 g^{-1}$, respectively. With those adsorption properties, these PAF materials could be considered as potential candidates for energetic gas adsorbents.

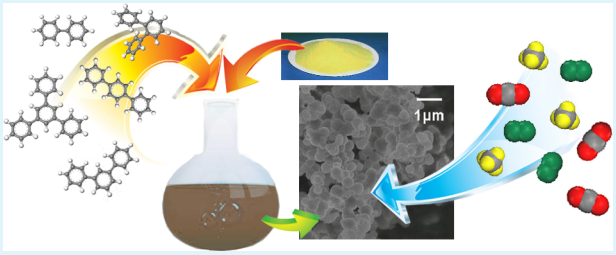

KEYWORDS: *porous organic framework, Scholl reaction, low-cost catalysts, commercial monomers, sole phenyl skeleton, gas adsorption*

INTRODUCTION

In host−guest chemistry, porous materials seem to be a superior platform with a considerable number of advantages as demonstrated recently.[1−4] In the past dozen years, porous organic frameworks (POFs) were introduced as promising members of the family of porous materials.[5−7] Their rigid structural networks and inherent porosities demonstrate excellent properties such as low density, high chemical and thermal stability, large specific surface areas (most importantly), etc.[8,9] Recently, a host of POFs were synthesized successfully by scientists all over the world, which greatly boosted the prosperity of porous materials.[10−12] Moreover, the potentials of these materials have been explored extensively, and it has been proven that they are of superiorities in terms of mechanical stability, gas adsorption, gas storage, heterogeneous catalysis, sensors, and electricity.[13−17]

Recently, the synthesis methods of POFs have also been extended to a great degree. Except for traditional classic reaction types,[18−22] researchers in this area also introduced a series of novel organic reactions into the field of POFs, for instance, polymer analogous reaction,[23] click reaction,[24,25] dibenzodioxane-forming reaction,[26] and Tröger's base polymerization reaction.[27] However, most of the routes mentioned above, both classic and novel ones, require either high-priced catalysts [e.g., palladium and nickel(0) compounds] or monomers with certain functional groups [e.g., Br, CHO, NH_2, $B(OH)_2$, etc.]. More importantly, the preparation of these monomers is still extremely complicated with multistep organic reactions and a tedious postprocess, as well as a large amount of financial investment.[28−31] On the basis of these facts, the cost of the synthesis of POFs is so great that it makes mass manufacturing difficult.

Besides the various reactions, selecting suitable building blocks is also an indispensable part of constructing POF materials. Commonly, the corresponding monomers are mainly of rigid and three-dimensional structures, for example, tetra(4-bromophenyl)methane, tetra[4-(dihydroxy)borylphenyl]-methane, etc.[9,32] However, the question of whether the functional groups and three-dimensional configuration are necessary remains.

In view of this situation, recently we have reported using the Scholl reaction to prepare PAF materials, without relying on complicated reactions, high-cost catalysts, or specific functional groups.[33] However, the building units of those experiments were still expensive three-dimensional monomers. Even with the advantage of inexpensive catalysts, the production of these PAFs still confronts another difficult challenge, the complex preparation of monomers and their high costs. In other words, the mass production of POF materials is restricted in terms of not only producing complexity but also selecting appropriate monomers, thereby making the development of a new strategy an urgent matter.

To obtain POFs with permanent pores, usually at least one of the monomers has to possess multifunctional activity sites. To the best of our knowledge, it has been very difficult to prepare porous polymers using only the linear monomers, but

Received: August 23, 2014
Accepted: December 12, 2014
Published: December 12, 2014

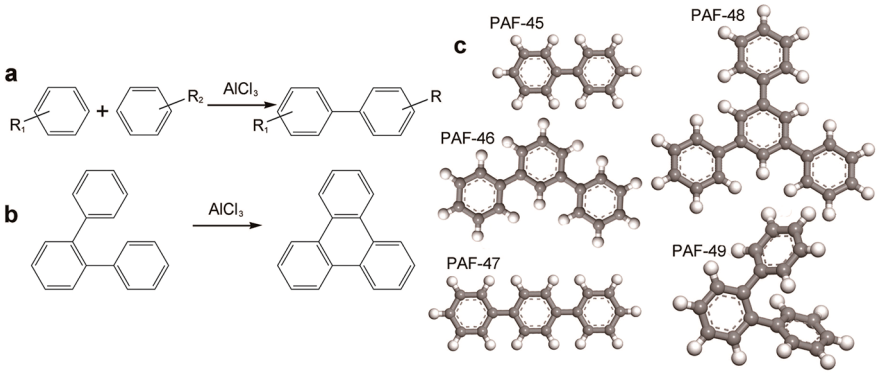

Figure 1. (a) Scholl reaction between molecules. (b) Possible cyclization within molecules, if the distance is appropriate. (c) Selected monomers for the construction of PAFs.

according to our experimental results, the phenyl rings can be coupled together at both the para position (major) and the ortho position (minor) to form polymeric networks during the Scholl reaction.[33] Inspired by that, we boldly selected linear and plane monomers, including biphenyl, *m*-terphenyl, *p*-terphenyl, 1,3,5-triphenylbenzene, and *o*-terphenyl, to construct PAF materials. These commercial chemicals possess the merit of price over other traditional POF monomers, bringing about possibilities for mass production and solving related social issues.

Today, environmental degeneration and traditional energy consumption have become challenges. They lead to numerous problems, including but not limited to adverse climate change, a decrease in total energy, and the rising price of fossil fuels. To solve these problems, utilizing clean and renewable energy and reducing greenhouse gas concentrations have become priorities. One of the excellent choices is to use renewable energy, for example, hydrogen and methane, whose power densities are 33.3 and 15.5 kW h kg^{-1}, respectively.[34,35] These sources are not only clean but also pollution-free. Currently, how to effectively transport and store highly flammable hydrogen and methane has become the main concern.[36] As for greenhouse effects, the massive emissions of carbon dioxide by traditional fuel combustion are the prime culprits evidenced in this regard. In fact, the concentration of CO_2 in the atmosphere is the highest among all the greenhouse gases and is responsible for approximately 60% of the global-warming effect.[37] Therefore, with increasing concern about energy and the environment, the attention of scientists turns to a search for appropriate candidates for H_2 and CH_4 carriers and CO_2 capture. Numerous adsorbents (MOFs, carbon materials, etc.[38−41]) with various porous textures have been investigated to satisfy the demand. As a hot topic research area of porous materials, POFs have become a promising star for gas storage, because of the many eye-catching points mentioned above, such as the sole composition of light elements, high stabilities even under air and moisture conditions, a large surface area, and structural controllability.[12,21,42,43]

Herein, we report a new cost-effective synthesis strategy for constructing PAF materials with commercial monomers and low-cost catalysts. These PAF materials, termed PAF-45, PAF-46, PAF-47, PAF-48, and PAF-49, were obtained with moderate BET surface areas ranging from 777 to 972 m^2 g^{-1}. The H_2, CO_2, and CH_4 sorption capacities of the resulting PAF materials were examined, and those gases exhibit unexpected performance. It is worth mentioning that PAF-49 shows excellent carbon dioxide and methane sorption, with values of 104 and 35 cm^3 g^{-1}, respectively. Also, all of these PAFs exhibit great H_2 sorption characteristics, ranging from 160 to 215 cm^3 g^{-1}. Given those adsorption properties, these POF materials could be considered as potential candidates for energetic gas adsorbents.

INSTRUMENTS AND MATERIALS

Biphenyl, *o*-terphenyl, *m*-terphenyl, 1,3,5-triphenylbenzene, and *p*-terphenyl were received from Aladdin Reagent in 99% purity. Chloroform was dried over 4 Å molecule sieves before being used. Other materials were purchased from commercial suppliers and used without further purification unless otherwise noted, and details of the types of instruments in this article can be found in the Supporting Information.

The syntheses of PAF-45, PAF-46, PAF-47, PAF-48, and PAF-49 were conducted under the same conditions described in our recent report.[33] The detailed synthesis procedures can be found in the Supporting Information.

RESULTS AND DISCUSSION

In syntheses of POFs, the effective polymerization reactions and suitable building blocks are two vital factors, which could determine their pore properties, skeletons, cost, and physical and chemical characteristics. Therefore, the development of polymerization reactions requires the exploration of economical catalysis, which could effectively decrease the cost of mass production. With regard to that, recently we explored a new method for preparing PAFs with a low-cost catalyst.[33] In this maneuverable and cheap strategy, the Lewis acid $AlCl_3$ facilitates aromatic coupling. When the cost factors of the monomers and catalysts were combined with the simplicity of the polymerization, the commercial linear and plane aromatic compounds were boldly selected as monomers. Specifically, the monomers in this study are biphenyl, *m*-terphenyl, *p*-terphenyl, 1,3,5-triphenylbenzene, and *o*-terphenyl. The phenyl rings are cross coupled together to form PAF materials, PAF-45, PAF-46, PAF-47, PAF-48, and PAF-49, respectively (Figure 1).

First, the Fourier transform infrared (FTIR) spectra were measured to identify the reaction process (Figure 2 and Figures S1 and S2 of the Supporting Information). After the Scholl reaction, the absorption peaks in the 1650−1400 cm^{-1} region and the 800−700 cm^{-1} region that belong to the C−H and C−C vibrations of the benzene ring obviously vary in terms of intensity. It is obvious that the intensity of infrared (IR) absorption of C−C becomes weaker, which could be attributed to the formation of polymeric networks that restrict the

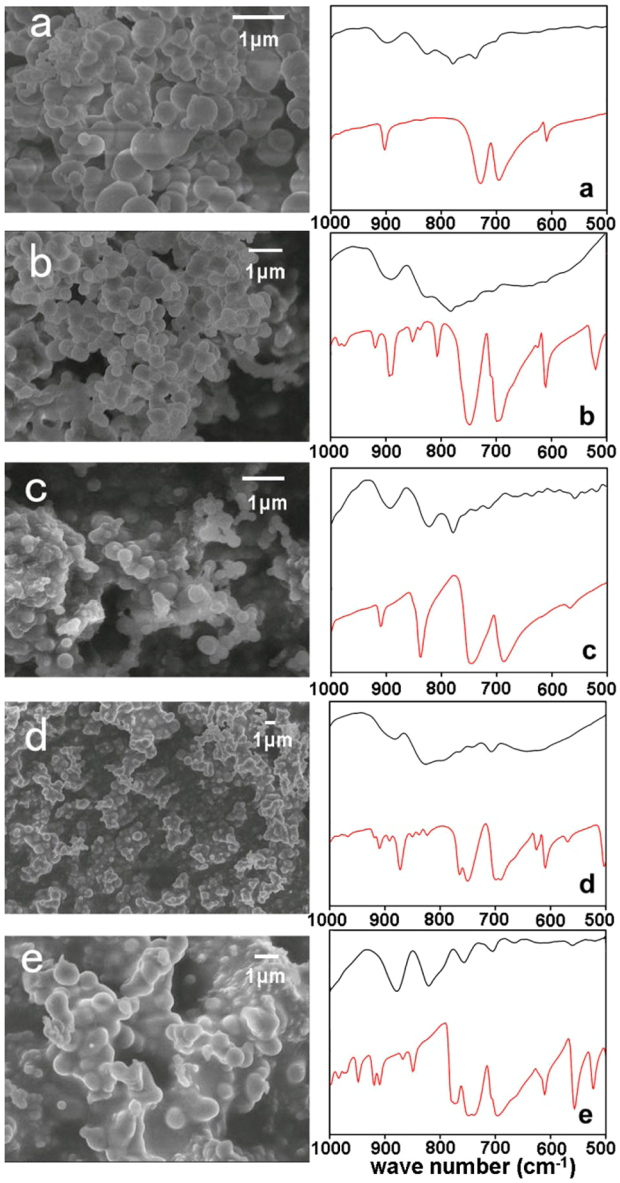

Figure 2. Scanning electron microscopy images (left) and infrared spectra (right, from 1000 to 500 cm^{-1}) of PAF-45 (a, black), PAF-46 (b), PAF-47 (c), PAF-48 (d), and PAF-49 (e). The data for the monomers are colored red, while those for the PAFs are colored black. The intensity of PAFs has all been enhanced doubly for the sake of clarity.

stretching and deformation vibration of molecules. Besides, values of C−H deformation of ring hydrogens are listed in Table S2 of the Supporting Information for clear illustration. In the initial monomers, C−H deformations could be classified as different kinds. For example, the peak at 732 cm^{-1} of biphenyl corresponds with five adjacent hydrogens, and the peaks at 747, 838, and 904 cm^{-1} of *m*-terphenyl correspond to four adjacent hydrogens, two adjacent hydrogens, and isolated hydrogen, respectively. Here PAF-45 and its monomer are selected as examples to demonstrate the reaction process, and the others are in a similar way. When the reaction occurred, the intensity of the peak at 732 cm^{-1} obviously became weaker (the C−H deformation vibration of five adjacent ring hydrogens), because of the reduction of adjacent ring hydrogens.

Besides, the C−H absorption peaks of PAF-45 extend from 730 to 910 cm^{-1}, including four adjacent hydrogen vibrations (770−730 cm^{-1}), three hydrogens (810−750 cm^{-1}), two hydrogens (860−800 cm^{-1}), and isolated hydrogen (910−860 cm^{-1}). There are three comparatively apparent peaks at 825, 780, and 738 cm^{-1}, which reveal the existence of two adjacent hydrogen vibrations, three hydrogens, and four hydrogens, respectively. This explains that the main substitution transpires at para, ortho, and meta positions. Furthermore, ring deformation vibration of monomers experienced a pronounced reduction in the intensity of the 715−690 cm^{-1} band due to the substitution of benzene rings. Thus, all this evidence demonstrates the occurrence between molecules and the possible formation of networks.

The local structures of these PAF materials were studied via solid-state ^{13}C CP/MAS nuclear magnetic resonance (NMR). As shown in Figure S3 of the Supporting Information, there are two main signal peaks in the range of 120−140 ppm, which could be attributed to aromatic carbon atoms of PAFs. As in previous reports, the signals at δ 128 could be assigned to unsubstituted phenyl carbons, while the signals at δ 142 are probably related to substituted phenyl carbons.[9] The visible peak at 55 ppm of PAF-46, PAF-47, and PAF-48 could be ascribed to remaining ethanol molecules according to the professional NMR appendix form (54.89 ppm), because ethanol is used in Soxhlet extraction to purify the products.

To investigate the morphology of the resulting PAF materials, scanning electron microscopy (SEM) (Figure 2 left) was employed. By that method, it is obvious that PAFs in this work afford a spherical morphology with diameters of 200−500 nm. Also, transmission electron microscopy (TEM) (shown in Figure S4 of the Supporting Information) was used to characterize the morphology and the pores of PAFs.

The crystallinity and regularity of these PAFs were investigated with the help of powder X-ray diffraction (PXRD) (in Figure S5 of the Supporting Information), which indicated their amorphous textures. It is difficult to form an ideal ordered structure among the building units in the actual frameworks, which is due to the distortion of phenyl rings and random substitution.

With regard to thermal stabilities, thermogravimetric analysis (TGA) was employed. As shown in Figure S6 of the Supporting Information, PAF-45 and PAF-49 barely lose any weight before 240 and 310 °C, respectively. Then, with the increase in temperature, the frameworks of PAF-45 and PAF-49 decompose gradually. As for PAF-46, PAF-47, and PAF-48, they show slow weight loss before 300 °C, and then the decomposition accelerates. Then the five PAF materials were tested with differential scanning calorimetry (DSC) (shown in Figure S7 of the Supporting Information). Through the experimental results, it is difficult to observe a certain glass transition temperature.

Chemical stability was tested by additional experiments. These polymers have been tested in solvents of high solubility (such as dimethylformamide, dimethyl sulfoxide, and *N*-methyl-2-pyrrolidone) and a 1 M HCl acid solution. In addition, they were purified via Soxhlet extraction using low-boiling point solvents ($CHCl_3$, THF, and CH_3CH_2OH). The experimental results show that PAFs in this work can neither be dissolved nor decomposed in any common solvents or solutions mentioned above, which demonstrates they are of great chemical stability. After the Soxhlet extraction, inductively coupled plasma mass spectrometry (ICP-MS) was also

dx.doi.org/10.1021/am505697f | ACS Appl. Mater. Interfaces 2015, 7, 201−208

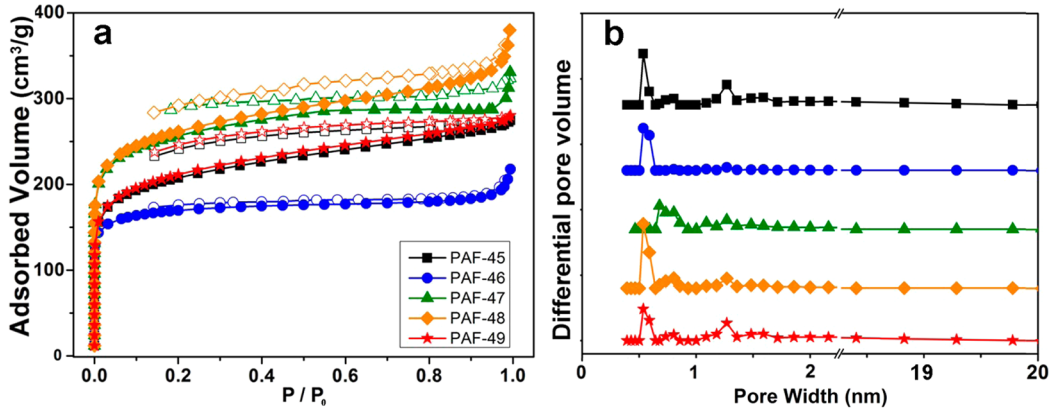

Figure 3. N_2 adsorption quantities (a) and pore width distributions (b) of PAF-45 (black), PAF-46 (blue), PAF-47 (olive), PAF-48 (orange), and PAF-49 (red). Filled symbols represent adsorption data while empty symbols desorption data.

Table 1. Porosity Data of the Five PAFs

	S_{BET} (m^2/g)	pore volume[a] (cm^3/g)	micropore volume[b] (cm^3/g)	mltramicropore volume[c] (cm^3/g)	micropore volume[d] (cm^3/g)	ultramicropore volume[e] (cm^3/g)
PAF-45	777	0.425	0.236	0.077	0.248	0.196
PAF-46	656	0.337	0.213	0.163	0.304	0.241
PAF-47	956	0.512	0.273	0.195	0.279	0.236
PAF-48	972	0.588	0.248	0.211	0.277	0.221
PAF-49	783	0.434	0.185	0.169	0.337	0.261

[a]Total pore volume calculated with N_2 adsorption results at a relative pressure P/P_0 of 0.99. [b]Cumulative pore volume calculated with N_2 adsorption results using the DFT model and a pore size of <2 nm. [c]Cumulative pore volume calculated with N_2 adsorption results using the DFT model and a pore size of <1 nm. [d]Cumulative pore volume calculated with CO_2 adsorption results and a pore size of <1.5 nm. [e]Cumulative pore volume calculated with CO_2 adsorption results and a pore size of <1.0 nm.

employed to measure catalyst residues in the PAFs, and according to the test results, the Al residues were all below 0.19 mg g^{-1}, demonstrating that the majority of the catalyst was removed (Table S1 of the Supporting Information).

Then, the nitrogen sorption isotherms at 77 K were tested to explore the porosities of these PAF materials. Before measurement, all samples were pumped to vacuum at 423 K for 6 h before the final measurement. According to Figure 3, PAF-46 shows a classic type I isotherm, while the N_2 uptakes of other PAFs sharply increase at the low-pressure region along with a steady linear increase at high relative pressure. In addition, there are distinct hystereses extending to the low-pressure region between the adsorption and desorption cycles, which is commonly presented in many POF networks. Their specific surface areas are calculated using the BET model (relative pressure P/P_0 = 0.03−0.10). The BET surface areas of all five materials exceed 650 m^2 g^{-1}, while that of PAF-48 reaches 972 m^2 g^{-1}. With regard to PAF-45 and PAF-47, if the phenyl rings of the corresponding monomers are coupled at only the para position, it is impossible for the obtained linear polymers to form porous textures (Figure S8 of the Supporting Information). In accord with the IR spectral data, the substitutions occurring at para, ortho, and meta positions are further proven by the results of N_2 sorption. Although the surface areas of these PAFs are not eye-catching, compared with other POFs, these materials are still not inferior to the others, especially considering their cost. To clarify, the comparisons, including the monomers, catalysts, and surface areas, are listed in Table S3 of the Supporting Information. Besides, the pore size distributions (psds) of these materials are calculated according to Density Functional Theory (DFT). It is clear that they show a narrow pore width of <1 nm, mainly at ∼0.56 nm. Only the PSD of PAF-47 is somewhat different (∼0.65 nm). One possible bold explanation is that the monomer that constitutes PAF-47 is the longest among all five monomers, ∼1.1 nm. Even though benzene ring in the middle also has the potential to participate in the phenyl coupling reaction, the skeleton units are still longer than the others.

As the pore volume is also an important parameter for porous materials, the total pore volumes of these PAFs are calculated from the results of N_2 adsorption. In addition, their ultramicropore and micropore volumes are also calculated with both 77 K N_2 adsorption and 273 K CO_2 adsorption (Figures S11 and S12 of the Supporting Information), yielding different results. These parameters can be found in Table 1.

Recently, Tan and co-workers also reported a novel synthesis method based on the Scholl reaction,[44] and the SMP-1 in that report shares the same monomer with PAF-48 and a similar experiment procedure. However, SMP-1 and PAF-48 exhibit different pore properties; for instance, the surface area of SMP-1 was ∼1254 m^2 g^{-1}. The difference may come from the sequence of adding ingredients and the uncertainty of the Scholl reaction. In the synthesis of SMP-1, the catalyst was added in the solution of $PhPh_3$, but when it came to PAF-48, the solution of the monomer was directly injected into an activated chloroform dispersion solution.

It has been documented that POFs with a narrow pore distribution (especially at pore sizes of <1 nm) could interact attractively with the gas molecules.[45,46] Besides, the amounts of benzene rings per unit volume also have a positive influence on the sorption properties.[47] Given the aromatic frameworks of PAF-45−PAF-49 together with the effect of small pores, the capabilities of PAFs with respect to the adsorption of energetic

dx.doi.org/10.1021/am505697f | ACS Appl. Mater. Interfaces 2015, 7, 201−208

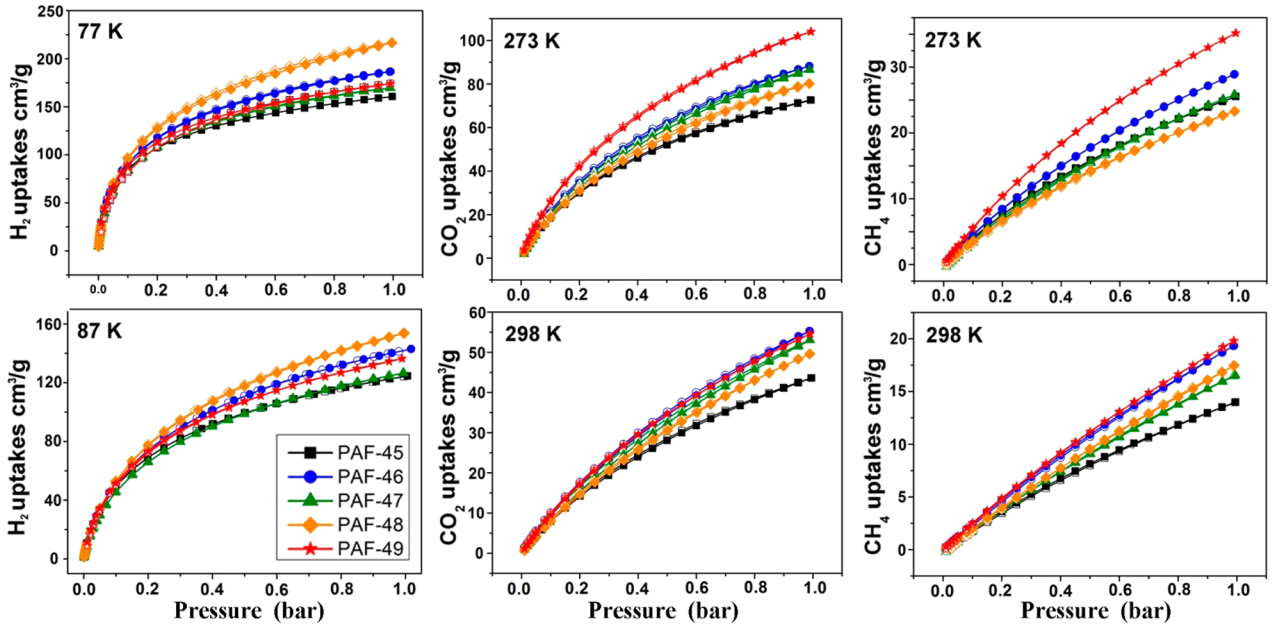

Figure 4. H_2, CO_2, and CH_4 adsorption isotherms for PAF-45 (black), PAF-46 (blue), PAF-47 (olive), PAF-48 (orange), and PAF-49 (red).

gases were studied. At 273 and 298 K, the CO_2 and CH_4 adsorptions were studied on these samples, while H_2 adsorptions were measured at 77 and 87 K. As expected, their microporous porosities provide them with an eye-catching arena in terms of H_2, CH_4, and CO_2 adsorptions.

According to Figure 4, the H_2 uptake of PAF-48 can reach 215 $cm^3\ g^{-1}$ (1.95 wt %) at 77 K, which is the highest among these samples. It is heartening to see that the other four PAF materials exhibit promising performance with respect to H_2 uptake, with the values exceeding 160 $cm^3\ g^{-1}$. Even the surface areas of PAFs range only from 655 to 972 $m^2\ g^{-1}$, and the H_2 uptakes of these PAFs are not inferior to those of other POF materials with larger surface areas. For example, PAF-1 with a BET surface area of 5600 $m^2\ g^{-1}$ possesses H_2 uptake of only 1.66 wt %, which is less than that of PAF-48 (215 $cm^3\ g^{-1}$, 1.95 wt %) and PAF-46 (187 $cm^3\ g^{-1}$, 1.67 wt %).[48] Compared with some respective porous materials, the samples used in this work also seem superior. At 77 K, MOF-5 with a BET surface area of 3000 $m^2\ g^{-1}$ shows less H_2 uptake: 1.30 wt % at 1.01 bar and 1.51 wt % at 1.13 bar.[49,50]

In addition, they exhibit great performance in CO_2 and CH_4 adsorptions, which are shown in Figure 4. Excitingly, at 273 K the CO_2 uptakes of all samples exceed 3.24 mmol g^{-1}, which are higher than most values of POFs. Among them, PAF-49 displays the best CO_2 results at 4.65 mmol g^{-1} (104.1 $cm^3\ g^{-1}$), which is among the leading positions of porous materials. For instance, it is significantly higher (3.47, 1.75, and 2.58 times) than those of COF-5, MOP-A, and CMP-1, while the BET surface area of PAF-49 is only 47.5, 19.2, and 89.7% of the surface areas of these materials, respectively.[51−53] A table comparing similar materials is given in Table S4 of the Supporting Information. In addition, in the area of CH_4 adsorption, all five materials have proven to be effective and impressive. At 273 K, the CH_4 uptakes of PAF-45−PAF-49 all exceed 1.14 mmol g^{-1}, especially that of PAF-49; its CH_4 adsorption quantity is 1.57 mmol g^{-1} (35.17 $cm^3\ g^{-1}$). Even with large surface areas, PAFs (PAF-1, PAF-3, and PAF-4) could hardly adsorb more than 1.21 mmol of methane g^{-1}.[48] Compared with other POFs listed in Table S4 of the Supporting Information, PAF-45−PAF-49 show excellent adsorption capacities; in particular, PAF-49 could be considered a promising adsorbent for CH_4 storage.

To determine a possibly reasonable explanation for their high gas uptakes, we have reviewed many reports and realized that gas adsorption behavior is a rather complicated process. From our perspective, the adsorption quantity of porous materials can be influenced by various factors, such as the pore size distribution (PSD), pore geometry, pore volumes, pore surface, etc.

It has been reported that N_2 adsorption at 77 K may not be completely exact for small pores. Because CO_2 molecules are linear instead of spherical and they can reach a range smaller than those of other gases, it is better to utilize the CO_2 adsorption results at 273 K to further characterize the details of narrow pores.[54] The PSDs of PAFs are shown in Figure 5, calculated through a nonlocal density functional theory (NLDFT) model with the official software from Quantachrome Instruments. The fitting comparison curves are shown in Figure S13 of the Supporting Information. There are some differences in the PSD between this one and the one calculated from N_2 adsorption. First, the details about <5 Å pores can be revealed.

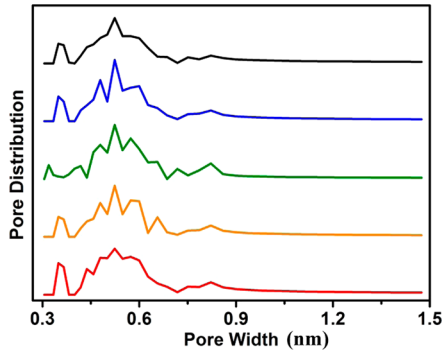

Figure 5. Pore distributions calculated with CO_2 adsorption isotherms for PAF-45 (black), PAF-46 (blue), PAF-47 (olive), PAF-48 (orange), and PAF-49 (red).

dx.doi.org/10.1021/am505697f | ACS Appl. Mater. Interfaces 2015, 7, 201−208

Table 2. CO_2, CH_4, and H_2 Uptake Data of the PAFs (P = 1.0 bar)

	CO_2 uptake[a] (cm^3/g)	CO_2 uptake[b] (cm^3/g)	CH_4 uptake[a] (cm^3/g)	CH_4 uptake[b] (cm^3/g)	H_2 uptake[c] (cm^3/g)	H_2 uptake[d] (cm^3/g)	$Q_{st}CO_2$ (kJ/mol)	$Q_{st}CH_4$ (kJ/mo)l	$Q_{st}H_2$ (kJ/mol)
PAF-45	73	44	26	14	161	125	28.8,	24.7	7.8
PAF-46	88	55	29	19	187	143	28.1	18.1	7.4
PAF-47	87	53	26	17	170	127	25.5	21.8	7.0
PAF-48	80	50	23	18	215	154	37.0	18.3	6.8
PAF-49	104	55	35	20	174	133	33.4	23.2	5.6

[a]T = 273 K. [b]T = 298 K. [c]T = 77 K. [d]T = 87 K.

For instance, it is easy to find out that there are existing pores at 3.4−4.0 Å, and this evidence may explain why PAF-49 and PAF-46 exhibit better CO_2 and CH_4 adsorption performance. As reported, the kinetic diameters of CO_2 and CH_4 are 0.34 and 0.38 nm, respectively.[55,56] From Figure 5, it is easy to find the pore distribution peaks of PAF-49 between 3.4 and 4.0 Å are the highest among those of all five PAF materials, which is consistent with the CO_2 adsorption results. As for PAF-46, although its surface area is the smallest, it indeed possesses the second highest pore distribution peak at 0.34−0.38 Å. The curved shapes and small molecule sizes of *m*-terphenyl and *o*-terphenyl make it easier to construct more slits, which is suitable for gas adsorption. As reported, storage capacity does not completely linearly correlate with surface area. Sometimes, pore sizes and their possible shapes can also be important factors.[57]

Via integration of the adsorption data measured at two different temperatures, the isosteric heats (Q_{st}) of the gases mentioned above are calculated to evaluate the affinity of PAFs with the software from Quantachrome Autosorb Co. (Figure S14 of the Supporting Information). Compared with those of other porous materials, the Q_{st} values of CH_4 and H_2 are moderate (Table 2). However, the Q_{st} of CO_2 is generally higher, indicated by the values of >25 kJ mol^{-1} even when CO_2 uptake reaches its maximum. The Q_{st} of CO_2 exceeds those of plenty of POFs, such as PAF-1 (15.6 kJ mol^{-1}), PAF-3 (19.2 kJ mol^{-1}), MOP-A (24.0 kJ mol^{-1}), COF-8 (24.8 kJ mol^{-1}), and COF-102 (16.54 kJ mol^{-1}).[32,48] It is worth mentioning that the Q_{st} value of PAF-49 remains stable for the whole coverage at approximately 33 kJ mol^{-1}.

Compared with reported POFs, PAF materials in this work, especially PAF-48 and -49, show relatively excellent adsorption properties. During careful analysis, the specific networks with pore widths of <1.0 nm in these PAFs could probably offer a perfect arena for gas molecule storage.

CONCLUSION

In summary, an extreme low-cost and easy construction strategy has been proposed for the construction of PAF materials. Combining them with our previous results for an inexpensive effective catalyst, we successfully synthesized a series of PAFs by using commercial chemicals. The structure, morphology, and porosity of these PAF products are comprehensively investigated by IR, NMR, XRD, SEM, and N_2 adsorption measurements. Although these PAFs display moderate surface areas ranging from 655 to 972 m^2 g^{-1}, they exhibit unexpected performance for H_2, CO_2, and CH_4 sorption capacities. It is worth mentioning that the H_2 uptake of PAF-48 reaches 215 cm^3 g^{-1}, and PAF-49 shows excellent carbon dioxide and methane sorption, with values of 104 and 35 cm^3 g^{-1}, respectively. What is also worth mentioning is that the strategy, using the affordable and readily available monomers as well as an inexpensive effective catalyst, could be employed for the mass production of POFs. This attempt provides promising opportunities for future application choices.

ASSOCIATED CONTENT

Supporting Information

FTIR spectra, TGA curves, powder X-ray diffraction, TEM images, and comparison of gas uptakes, isosteric heats of adsorption, DSC curves, fitting comparison curves, cumulative pore volumes, etc. This material is available free of charge via the Internet at http://pubs.acs.org.

AUTHOR INFORMATION

Corresponding Author

*E-mail: renhao@jlu.edu.cn.

Author Contributions

L.L. and H.R. designed and engineered the samples. L.L. wrote the paper with support from H.R. K.C. performed the gas adsorption experiments and collected the data. P.W. performed the SEM experiments and collected the data. G.Z. and H.R. performed the data analysis and theoretical analysis. All authors contributed to the general discussion.

Notes

The authors declare no competing financial interest.

ACKNOWLEDGMENTS

We are grateful for the financial support from the National Basic Research Program of China (973 Program, Grants 2012CB821700 and 2014CB931800), the Major International (Regional) Joint Research Project of the National Science Foundation of China (Grant 21120102034), and National Science Foundation of China (Grant 21201074).

REFERENCES

(1) Feng, X.; Ding, X.; Jiang, D. Covalent Organic Frameworks. *Chem. Soc. Rev.* **2012**, *41*, 6010−6022.
(2) Long, J. R.; Yaghi, O. M. The Pervasive Chemistry of Metal-Organic Frameworks. *Chem. Soc. Rev.* **2009**, *38*, 1213−1214.
(3) Zou, X.; Ren, H.; Zhu, G. Topology-directed Design of Porous Organic Frameworks and their Advanced Applications. *Chem. Commun.* **2013**, *49*, 3925−3936.
(4) Li, Y.; Yu, J. New Stories of Zeolite Structures: Their Descriptions, Determinations, Predictions, and Evaluations. *Chem. Rev.* **2014**, *114*, 7268−7316.
(5) Vilela, F.; Zhang, K.; Antonietti, M. Conjugated Porous Polymers for Energy Applications. *Energy Environ. Sci.* **2012**, *5*, 7819−7832.
(6) Ding, S.-Y.; Wang, W. Covalent Organic Frameworks (COFs): From Design to Applications. *Chem. Soc. Rev.* **2013**, *42*, 548−568.
(7) Cooper, A. I. Covalent Organic Frameworks. *CrystEngComm* **2013**, *15*, 1483−1483.
(8) Wu, D.; Xu, F.; Sun, B.; Fu, R.; He, H.; Matyjaszewski, K. Design and Preparation of Porous Polymers. *Chem. Rev.* **2012**, *112*, 3959−4015.

(9) Ben, T.; Ren, H.; Ma, S.; Cao, D.; Lan, J.; Jing, X.; Wang, W.; Xu, J.; Deng, F.; Simmons, J. M. Targeted Synthesis of a Porous Aromatic Framework with High Stability and Exceptionally High Surface Area. *Angew. Chem.* **2009**, *121*, 9621−9624.
(10) Sui, Z.-Y.; Cui, Y.; Zhu, J.-H.; Han, B.-H. Preparation of Three-Dimensional Graphene Oxide-Polyethylenimine Porous Materials as Dye and Gas Adsorbents. *ACS Appl. Mater. Interfaces* **2013**, *5*, 9172−9179.
(11) Weston, M. H.; Colón, Y. J.; Bae, Y.-S.; Garibay, S. J.; Snurr, R. Q.; Farha, O. K.; Hupp, J. T.; Nguyen, S. T. High Propylene/propane Adsorption Selectivity in a Copper (catecholate)-decorated Porous Organic Polymer. *J. Mater. Chem. A* **2014**, *2*, 299−302.
(12) Zhao, Y.; Yao, K. X.; Teng, B.; Zhang, T.; Han, Y. A Perfluorinated Covalent Triazine-based Framework for Highly Selective and Water-tolerant CO_2 Capture. *Energy Environ. Sci.* **2013**, *6*, 3684−3692.
(13) Wang, X.-S.; Liu, J.; Bonefont, J. M.; Yuan, D.-Q.; Thallapally, P. K.; Ma, S. A Porous Covalent Porphyrin Framework with Exceptional Uptake Capacity of Saturated Hydrocarbons for Oil Spill Cleanup. *Chem. Commun.* **2013**, *49*, 1533−1535.
(14) Zhou, D.; Wu, H.; Wei, Z.; Han, B.-H. Graphene-molybdenum Oxynitride Porous Material with Improved Cyclic Stability and rate capability for Rechargeable Lithium ion Batteries. *Phys. Chem. Chem. Phys.* **2013**, *15*, 16898−16906.
(15) Zhang, Y.; Riduan, S. N. Functional Porous Organic Polymers for Heterogeneous Catalysis. *Chem. Soc. Rev.* **2012**, *41*, 2083−2094.
(16) Woodward, R. T.; Stevens, L. A.; Dawson, R.; Vijayaraghavan, M.; Hasell, T.; Silverwood, I. P.; Ewing, A. V.; Ratvijitvech, T.; Exley, J. D.; Chong, S. Y. Swellable, Water- and Acid-Tolerant Polymer Sponges for Chemoselective Carbon Dioxide Capture. *J. Am. Chem. Soc.* **2014**, *136*, 9028−9035.
(17) Tanabe, K. K.; Siladke, N. A.; Broderick, E. M.; Kobayashi, T.; Goldston, J. F.; Weston, M. H.; Farha, O. K.; Hupp, J. T.; Pruski, M.; Mader, E. A. Stabilizing Unstable Species through Single-site Isolation: A Catalytically active Ta^V trialkyl in a Porous Organic Polymer. *Chem. Sci.* **2013**, *4*, 2483−2489.
(18) Zhang, Y.-B.; Su, J.; Furukawa, H.; Yun, Y.; Gándara, F.; Duong, A.; Zou, X.; Yaghi, O. M. Single-Crystal Structure of a Covalent Organic Framework. *J. Am. Chem. Soc.* **2013**, *135*, 16336−16339.
(19) Li, B.; Zhang, Y.; Krishna, R.; Yao, K.; Han, Y.; Wu, Z.; Ma, D.; Shi, Z.; Pham, T.; Space, B. Introduction of π-Complexation into Porous Aromatic Framework for Highly Selective Adsorption of Ethylene over Ethane. *J. Am. Chem. Soc.* **2014**, *136*, 8654−8660.
(20) Lu, W.; Wei, Z.; Yuan, D.; Tian, J.; Fordham, S.; Zhou, H.-C. Rational Design and Synthesis of Porous Polymer Networks: Toward High Surface Area. *Chem. Mater.* **2014**, *26*, 4589−4597.
(21) Xu, Y.; Jin, S.; Xu, H.; Nagai, A.; Jiang, D. Conjugated Microporous Polymers: Design, Synthesis and Application. *Chem. Soc. Rev.* **2013**, *42*, 8012−8031.
(22) Jing, X.; Sun, F.; Ren, H.; Tian, Y.; Guo, M.; Li, L.; Zhu, G. Targeted Synthesis of Micro−mesoporous Hybrid Material Derived from Octaphenylsilsesquioxane Building Units. *Microporous Mesoporous Mater.* **2013**, *165*, 92−98.
(23) Thiel, K.; Zehbe, R.; Roeser, J.; Strauch, P.; Enthaler, S.; Thomas, A. A Polymer Analogous Reaction for the Formation of Imidazolium and NHC Based Porous Polymer Networks. *Polym. Chem.* **2013**, *4*, 1848−1856.
(24) Xie, L. H.; Suh, M. P. High CO_2-Capture Ability of a Porous Organic Polymer Bifunctionalized with Carboxy and Triazole Groups. *Chem.—Eur. J.* **2013**, *19*, 11590−11597.
(25) Holst, J. R.; Stöckel, E.; Adams, D. J.; Cooper, A. I. High Surface Area Networks from Tetrahedral Monomers: Metal-Catalyzed Coupling, Thermal Polymerization, and "Click" Chemistry. *Macromolecules* **2010**, *43*, 8531−8538.
(26) Budd, P. M.; Elabas, E. S.; Ghanem, B. S.; Makhseed, S.; McKeown, N. B.; Msayib, K. J.; Tattershall, C. E.; Wang, D. Solution-Processed, Organophilic Membrane Derived from a Polymer of Intrinsic Microporosity. *Adv. Mater.* **2004**, *16*, 456−459.
(27) Carta, M.; Malpass-Evans, R.; Croad, M.; Rogan, Y.; Jansen, J. C.; Bernardo, P.; Bazzarelli, F.; McKeown, N. B. An Efficient Polymer Molecular Sieve for Membrane Gas Separations. *Science* **2013**, *339*, 303−307.
(28) Yan, Z.; Ren, H.; Ma, H.; Yuan, R.; Yuan, Y.; Zou, X.; Sun, F.; Zhu, G. Construction and Sorption Properties of Pyrene-Based Porous Aromatic Frameworks. *Microporous Mesoporous Mater.* **2013**, *173*, 92−98.
(29) Yuan, Y.; Sun, F.; Zhang, F.; Ren, H.; Guo, M.; Cai, K.; Jing, X.; Gao, X.; Zhu, G. Targeted Synthesis of Porous Aromatic Frameworks and their Composites for Versatile, Facile, Efficacious, and Durable Antibacterial Polymer Coatings. *Adv. Mater.* **2013**, *25*, 6619−6624.
(30) Ren, H.; Ben, T.; Sun, F.; Guo, M.; Jing, X.; Ma, H.; Cai, K.; Qiu, S.; Zhu, G. Synthesis of a Porous Aromatic Framework for Adsorbing Organic Pollutants Application. *J. Mater. Chem.* **2011**, *21*, 10348−10353.
(31) Ma, H.; Ren, H.; Zou, X.; Sun, F.; Yan, Z.; Cai, K.; Wang, D.; Zhu, G. Novel Lithium-loaded Porous Aromatic Framework for Efficient CO_2 and H_2 Uptake. *J. Mater. Chem. A* **2013**, *1*, 752−758.
(32) El-Kaderi, H. M.; Hunt, J. R.; Mendoza-Cortés, J. L.; Côté, A. P.; Taylor, R. E.; O'Keeffe, M.; Yaghi, O. M. Designed Synthesis of 3D Covalent Organic Frameworks. *Science* **2007**, *316*, 268−272.
(33) Li, L.; Ren, H.; Yuan, Y.; Yu, G.; Zhu, G. Construction and Adsorption Properties of Porous Aromatic Frameworks via $AlCl_3$-triggered Coupling Polymerization. *J. Mater. Chem. A* **2014**, *2*, 11091−11098.
(34) Schlapbach, L.; Züttel, A. Hydrogen-storage Materials for Mobile Applications. *Nature* **2001**, *414*, 353−358.
(35) Han, S. S.; Mendoza-Cortés, J. L.; Goddard Iii, W. A. Recent advances on Simulation and Theory of Hydrogen Storage in Metal-Organic Frameworks and Covalent Organic Frameworks. *Chem. Soc. Rev.* **2009**, *38*, 1460−1476.
(36) Ogden, J. M. Prospects for Building a Hydrogen Energy Infrastructure. *Annu. Rev. Energy* **1999**, *24*, 227−279.
(37) Yang, H.; Xu, Z.; Fan, M.; Gupta, R.; Slimane, R. B.; Bland, A. E.; Wright, I. Progress in Carbon Dioxide Separation and Capture: A review. *J. Environ. Sci.* **2008**, *20*, 14−27.
(38) Chu, S. Carbon Capture and Sequestration. *Science* **2009**, *325*, 1599−1599.
(39) Lu, W.; Yuan, D.; Sculley, J.; Zhao, D.; Krishna, R.; Zhou, H.-C. Sulfonate-grafted Porous Polymer Networks for Preferential CO_2 Adsorption at Low Pressure. *J. Am. Chem. Soc.* **2011**, *133*, 18126−18129.
(40) Babarao, R.; Dai, S.; Jiang, D.-e. Functionalizing Porous Aromatic Frameworks with Polar Organic Groups for High-Capacity and Selective CO_2 Separation: A Molecular Simulation Study. *Langmuir* **2011**, *27*, 3451−3460.
(41) Kandambeth, S.; Mallick, A.; Lukose, B.; Mane, M. V.; Heine, T.; Banerjee, R. Construction of Crystalline 2D Covalent Organic Frameworks with Remarkable Chemical (acid/base) Stability via a Combined Reversible and Irreversible Route. *J. Am. Chem. Soc.* **2012**, *134*, 19524−19527.
(42) Petrášová, S.; Zukal, A.; Brus, J.; Balcar, H.; Pastva, J.; Zedník, J.; Sedláček, J. New Hyper-Crosslinked Partly Conjugated Networks with Tunable Composition by Spontaneous Polymerization of Ethynylpyridines with Bis(bromomethyl) arenes: Synthesis, Spectral Properties, and Activity in CO_2 Capture. *Macromol. Chem. Phys.* **2013**, *214*, 2856−2866.
(43) Garibay, S. J.; Weston, M. H.; Mondloch, J. E.; Colón, Y. J.; Farha, O. K.; Hupp, J. T.; Nguyen, S. T. Accessing Functionalized Porous Aromatic Frameworks (PAFs) through a de novo approach. *CrystEngComm* **2013**, *15*, 1515−1519.
(44) Li, B.; Guan, Z.; Yang, X.; Wang, W. D.; Wang, W.; Hussain, I.; Song, K.; Tan, B.; Li, T. Multifunctional Microporous Organic Polymers. *J. Mater. Chem. A* **2014**, *2*, 11930−11939.
(45) Zhu, Y.; Long, H.; Zhang, W. Imine-Linked Porous Polymer Frameworks with High Small Gas (H_2, CO_2, CH_4, C_2H_2) Uptake and CO_2/N_2 Selectivity. *Chem. Mater.* **2013**, *25*, 1630−1635.

(46) Chen, Q.; Luo, M.; Hammershøj, P.; Zhou, D.; Han, Y.; Laursen, B. W.; Yan, C.-G.; Han, B.-H. Microporous Polycarbazole with High Specific Surface Area for Gas Storage and Separation. *J. Am. Chem. Soc.* **2012**, *134*, 6084−6087.
(47) Wu, H.; Simmons, J. M.; Liu, Y.; Brown, C. M.; Wang, X. S.; Ma, S.; Peterson, V. K.; Southon, P. D.; Kepert, C. J.; Zhou, H. C. Metal-Organic Frameworks with Exceptionally High Methane Uptake: Where and How is Methane Stored? *Chem.—Eur. J.* **2010**, *16*, 5205−5214.
(48) Ben, T.; Pei, C.; Zhang, D.; Xu, J.; Deng, F.; Jing, X.; Qiu, S. Gas Storage in Porous Aromatic Frameworks (PAFs). *Energy Environ. Sci.* **2011**, *4*, 3991−3999.
(49) Rowsell, J. L.; Spencer, E. C.; Eckert, J.; Howard, J. A.; Yaghi, O. M. Gas Adsorption Sites in a Large-pore Metal-Organic Framework. *Science* **2005**, *309*, 1350−1354.
(50) Kaye, S. S.; Dailly, A.; Yaghi, O. M.; Long, J. R. Impact of Preparation and Handling on the Hydrogen Storage Properties of Zn_4O(1,4-benzenedicarboxylate)$_3$ (MOF-5). *J. Am. Chem. Soc.* **2007**, *129*, 14176−14177.
(51) Dawson, R.; Adams, D. J.; Cooper, A. I. Chemical Tuning of CO_2 Sorption in Robust Nanoporous Organic Polymers. *Chem. Sci.* **2011**, *2*, 1173−1177.
(52) Furukawa, H.; Yaghi, O. M. Storage of Hydrogen, Methane, and Carbon Dioxide in Highly Porous Covalent Organic Frameworks for Clean Energy Applications. *J. Am. Chem. Soc.* **2009**, *131*, 8875−8883.
(53) Dawson, R.; Stöckel, E.; Holst, J. R.; Adams, D. J.; Cooper, A. I. Microporous Organic Polymers for Carbon Dioxide Capture. *Energy Environ. Sci.* **2011**, *4*, 4239−4245.
(54) Lozano-Castello, D.; Cazorla-Amoros, D.; Linares-Solano, A. Usefulness of CO_2 Adsorption at 273 K for the Characterization of Porous Carbons. *Carbon* **2004**, *42*, 1233−1242.
(55) D'Alessandro, D. M.; Smit, B.; Long, J. R. Carbon Dioxide Capture: Prospects for New Materials. *Angew. Chem., Int. Ed.* **2010**, *49*, 6058−6082.
(56) Li, S.; Falconer, J. L.; Noble, R. D. Improved SAPO-34 Membranes for CO_2/CH_4 Separations. *Adv. Mater.* **2006**, *18*, 2601−2603.
(57) Gogotsi, Y.; Portet, C.; Osswald, S.; Simmons, J. M.; Yildirim, T.; Laudisio, G.; Fischer, J. E. Importance of Pore Size in High-Pressure Hydrogen Storage by Porous Carbons. *Int. J. Hydrogen Energy* **2009**, *34*, 6314−6319.